Lifetimes of confined optical phonons and the shape of a Raman peak in disordered nanoparticles. I. Analytical treatment

Oleg I. Utesov [1,2,*] Andrey G. Yashenkin,[1,2] and Sergei V. Koniakhin [3,4,†]

[1] *Petersburg Nuclear Physics Institute NRC "Kurchatov Institute", Gatchina 188300, Russia*

[2] *Department of Physics, St. Petersburg State University, St. Petersburg 199034, Russia*

[3] *Institute Pascal, PHOTON-N2, University Clermont Auvergne, CNRS, 4 Avenue Blaise Pascal, Aubière Cedex 63178, France*

[4] *St. Petersburg Academic University - Nanotechnology Research and Education Centre of the Russian Academy of Sciences, St. Petersburg 194021, Russia*

(Received 16 July 2020; accepted 22 October 2020; published 16 November 2020)

Microscopic description of Raman spectra in nanopowders of nonpolar crystals is accomplished by developing the theory of disorder-induced broadening of optical vibrational eigenmodes. Analytical treatment of this problem is performed, and line shape and width are determined as functions of phonon quantum numbers, nanoparticle shape, size, and the strength of disorder. The results are found to be strongly dependent on whether the broadened line is separated from or overlaps other lines of the spectrum. Three models of disorder, i.e., weak pointlike impurities, weak smooth random potential, and strong rare impurities, are investigated in detail. The possibility of forming the phonon-impurity bound state is also studied.

DOI: 10.1103/PhysRevB.102.205421

I. INTRODUCTION

The properties of very small particles and their ensembles are a subject of current active scientific investigation, mostly due to their promising applications in materials science [1], quantum computing [2–4], chemistry [5,6], biology and medicine [7–10], etc. Among others, disordered arrays (powders and water suspensions) of crystalline nanoparticles of nonpolar crystals, both semiconducting and diamond-like ones, attract close attention.

Even before being utilized in a certain manner, the nanopowders need to be attested and certified. For comprehensive certification of a powder such obvious characteristics as chemical formula and crystallographic structure of the material that form particles of a powder should be supplemented by geometrical parameters of its constituents such as (i) the mean size of a particle, (ii) the particle size distribution function, (iii) the effective faceting number (in the case of nontrivial particle shape), and (iv) the measure of their elongation (if exists), as well as by some characteristics of (v) nanoparticle intrinsic disorder, surface morphology, and phase composition.

In order to examine the nanopowders, several experimental techniques are utilized. High-resolution transmission electron microscopy (HRTEM) [11–17], atomic force microscopy (AFM) [13,14,18], dynamical light scattering [19–22], x-ray diffraction [17,23,24], and Raman spectroscopy (see, e.g., Ref. [25] and references therein) are among them. The latter one is of prime importance because it provides a unique precise and nondestructive tool for optical investigation of collective excitations in nanoparticles. Examining the shape of a Raman peak and its position one could extract a great amount of information about the nanoparticles including some parameters mentioned above [26,27].

Indeed, since the momentum in a particle is quantized due to the finite-size quantization effect, the maximum of a Raman peak for nanoparticles is redshifted (i.e., shifted to lower frequency) as compared to the bulk material, with the shift value increasing for smaller particles. Furthermore, the entire discrete spectrum of vibrational modes for the particle of a given shape is peculiar and specific for this particular shape [26,27]. This manifests itself in the asymmetry of the Raman peak. One can think of restoring the *portrait* of a particle from the analysis of the peak shape and its position, thus formulating a sort of "inverse problem." It makes the Raman data analysis a very important and challenging issue. The goal of this work is to present an instrument for this analysis in the form of a microscopic theory of Raman scattering in nanoparticles which includes intrinsic disorder as the main mechanism of phonon damping.

Recently, we proposed two closely related methods of the Raman data evaluation [26,27] which gave much more detailed information about the parameters of a powder than all previously used variations of the phonon confinement model (PCM) [28–33] and other models [34,35] provided. One of these methods, the dynamical matrix method–bond polarization model (DMM-BPM) [26], consists of the direct solving of the dynamical matrix eigenproblem [36] for a particle with further evaluation of its Raman spectrum. The latter procedure utilizes the proportionality between the electric polarization and the deformation in nonpolar crystals with the use of the bond polarization model [37]. The (empirically broadened) individual lines of the spectrum together constitute the first (and subsequent) Raman peaks [26].

*utiosov@gmail.com

†kon@mail.ioffe.ru

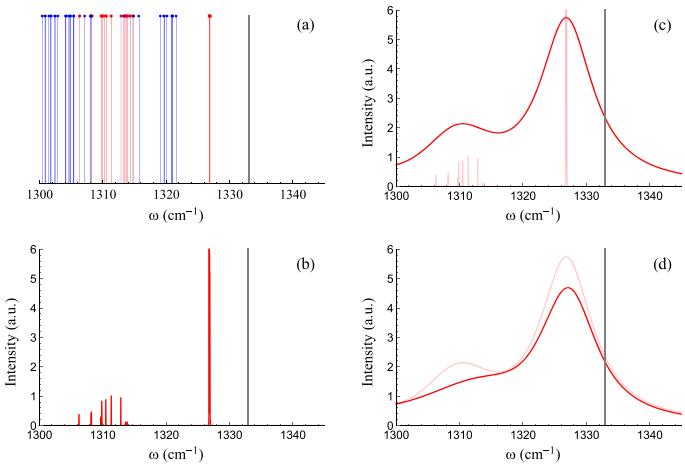

FIG. 1. Four steps necessary to obtain the Raman peak for a diamond nanopowder. Gray vertical line marks the maximal optical phonon frequency ω_0. (a) The phonon spectrum of a 3 nm cubic diamond particle consists of Raman-active (red) and Raman-silent (blue) modes. (b) The Raman spectrum before broadening; only Raman-active modes contribute. (c) Phenomenologically broadened Raman spectrum is a smooth function with the main and subsequent peaks. (d) The Raman spectrum of a powder with the mean particle size 3 nm and the standard deviation 0.3 nm. Only the main Raman peak is clearly seen while subsequent peaks are smeared out into the slightly sloping left shoulder. In (c) and (d) the results of the respective previous steps are shown by semitransparent color. The main goal of the present work is to establish microscopic grounds for individual phonon line broadening procedure.

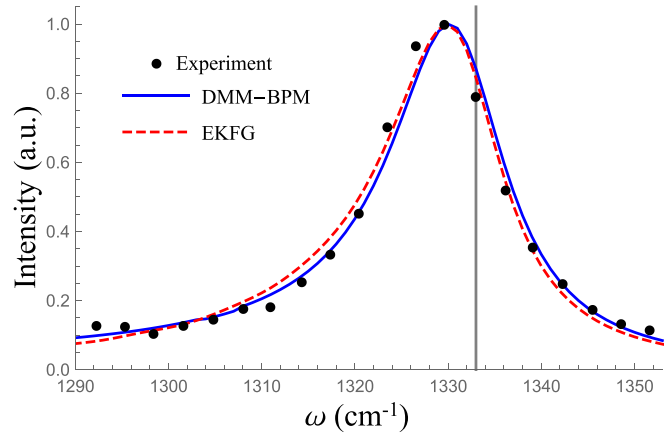

FIG. 2. DMM-BPM and EKFG approaches both successfully interpret experimental data. Here the solid blue curve (DMM-BPM) and the dashed red curve (EKFG) stand for the best fit of the experimental Raman spectrum of nanodiamond powder from Ref. [13] (black dots); the only free parameter is the phonon linewidth Γ. The vertical gray line represents the maximal optical phonon frequency in the bulk ω_0.

An important observation made in Ref. [26] and related to the discrete spectra of nanoparticles (before this broadening is done) concerns their fine structure shared by all particle shapes investigated. Namely, the spectrum starts from a threefold-degenerate first line which carries the majority (more than 2/3) of its weight. This triple line is well separated from the rest of the spectrum that begins effectively with the 13th line because of dividing the eigenmodes onto "Raman active" and "Raman silent" ones. The Raman-silent modes do not contribute to the Raman spectra due to the symmetry properties of their eigenfunctions. Furthermore, both types of modes form a "quasicontinuum" wherein the level spacings are essentially smaller than the first gap. This quasicontinuum is split onto several "bands" by inter-band-gaps which do not exceed the first one [see Fig. 1(a)].

Terminologically, we shall distinguish between (i) the phonon lines that form the vibrational spectrum of a nanoparticle [see Fig. 1(a)], (ii) the Raman spectrum which includes only the Raman active modes with corresponding weights influenced by the photon-phonon scattering matrix elements [see Fig. 1(b)], and (iii) the main (and possibly subsequent) Raman peak constituted by broadened Raman spectrum lines [see Fig. 1(c)] of all the particle sizes contained in a powder [see Fig. 1(d)].

Another proposed method replaces the original discrete dynamical matrix problem with its long-wavelength continuous counterpart which is the Euclidian Klein-Fock-Gordon equation under the Dirichlet boundary conditions [27]; we dub this approach "EKFG." Being supplemented by the continuous version of the bond polarization model and by the phenomenological line broadening procedure this approach generates the Raman spectra almost indistinguishable from those obtained within the DMM-BPM scheme, although *before* the line broadening the EKFG spectra look a bit oversimplified as compared to the DMM-BPM ones: they contain only one degenerate level in the place where the DMM-BPM method yields many weakly split levels, etc.

This means that the EKFG method correctly captures a spectral weight distribution along the energy axis rather than all rigorous details of the spectrum. Since the spectral line broadening plays the role of an effective energy averaging, the approximate EKFG method appears to be sufficient for reproducing all important features of such integral characteristics as the first Raman peak; see Fig. 2.

The imperfection of these theories [26,27] is the phenomenological character of the line-broadening procedure; the linewidth parameter Γ is treated as a fitting one with no theoretical analysis of its origin and value. To the best of our knowledge, no detailed theory of the Raman peak broadening in nanoparticles exists in modern literature; all current attempts have mostly phenomenological or philological character. (One should mention the paper by Yoshikawa *et al.* [38] who extracted $\Gamma \propto \text{constant} + 1/L$ dependence, with L being the particle size, from the analysis of experimental data.) The present work aims to accomplish the approach of Refs. [26,27], providing us with the microscopic theory of the Raman peak broadening due to nanoparticle *disorder and imperfections*, as well as with its numerical verification.

The work consists of two papers, and this is the first one (hereinafter, paper I). Within the framework of a set of simple models of disorder it analytically treats the linewidth problem in disordered nanoparticles. The second paper (Ref. [39]; hereinafter, paper II) is devoted to numerical simulations of the same problem, necessary for both verification and justification of the analytical results of paper I, as well as for

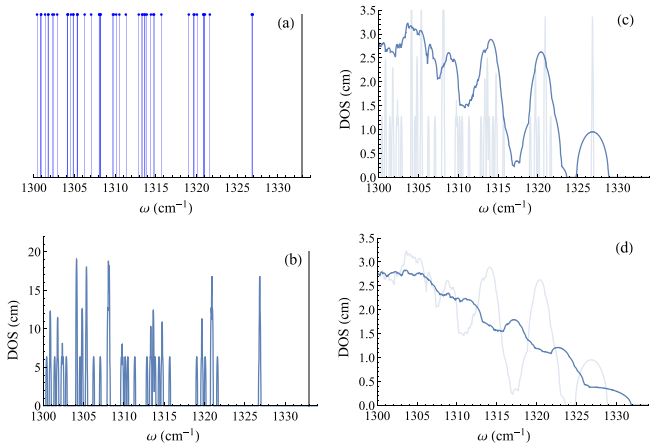

FIG. 3. The phonon spectrum of a 3 nm cubic nanodiamond calculated with the use of the DMM-BPM approach for several amounts of disorder; the position of the bulk phonon peak is marked by the black vertical line. (a) Clean case. Each dot corresponds to certain eigenfrequency. (b) For the weakest disorder the density of states (DOS) consists of discrete peaks. (c) For stronger disorder the lines in quasicontinuum begin to overlap, whereas the first triple mode is still separated. (d) For the strongest disorder all the modes are overlapped and the DOS is getting close to the bulk one. In (c) and (d) the results of the respective previous plots for weaker disorder are shown by semitransparent color.

numerical investigation of disorder types and regimes which are hardly analyzable analytically. In line with paper I, the numerical paper II allows us to represent the all-around picture of the dirty Raman problem including the effect of realistic disorder.

In order to get a preliminary insight into our theory and to understand better the general picture we propose, let us discuss in detail Fig. 3. Panel (a) represents the typical spectrum of vibrational optical eigenmodes of a particle. As we said above, this spectrum consists of the threefold-degenerate first line and a sequence of "bands," the interlevel distances between the lines in these bands being essentially smaller than the first gap. Then we introduce disorder into the system. For a small amount of disorder it broadens the spectral lines, see Fig. 3(b), but the lines remain narrower than the distances between the levels. This is valid for levels lying inside the bands as well as for the first (triple) line. Therefore, we are in the regime of separated levels now for all parts of the spectrum. With disorder increasing, the levels inside the bands start to overlap, while the first line is still separated from the rest of the spectrum; see Fig. 3(c). Hence, for this amount of disorder the band levels cross over to the continuous regime, while the first triple line remains in the discrete one. We argue that this "mixed" situation is typical for nanoparticles that have the size of the order of several nanometers which were investigated in recent experiments [14]. At last, with the further increase of disorder the linewidths become so large that they fill in even the first (largest) gap, making the entire spectrum continuous; see Fig. 3(d).

We presented above this detailed picture of the line broadening in order to highlight the importance of the main statement of the present work (which, however, sounds quite evident from a general point of view). Namely, we argue that *the properties of the phonon linewidths in nanoparticles vary dramatically depending on whether the level is a separated level or whether it belongs to the continuum.*

More specifically, in paper I we study *analytically* the phonon scattering by weak pointlike impurities. For the disorder-induced broadening of spectral lines we observe the linear dependence on the disorder strength parameter S and the inverse proportionality to the mean particle size L, $\Gamma \propto S/L$, when the broadened levels are overlapped. For separated levels the linewidths behave as $\Gamma \propto \sqrt{S}/L^{3/2}$. At fixed impurity strength there exists a crossover particle size $\mathcal{L}_c \propto a_0 S^{-1}$ between these two regimes. The strength parameter S is defined as a product of the (dimensionless) impurity concentration $c_{\rm imp}$ and the (squared normalized) variation of a random parameter of the theory (here, the atomic mass m), which yields $S = c_{\rm imp}(\delta m/m)^2$, with a_0 being the lattice constant. The prefactors in both regimes are found to be specifically phonon quantum number n and faceting number p dependent quantities; the latter serves for shape parametrization purposes (elongated particles are not considered). We also detect the non-Lorentzian shapes of spectral lines in the separated regime of level broadening and a strong line shape asymmetry in the overlapped regime.

Examining then the lowest eigenmodes of phonons subjected to a smooth random impurity potential we find that the results crucially depend on the relationship between the mean particle size L and the characteristic spatial scale of a random potential σ. At $\sigma < L$ the formulas obtained for pointlike impurities are also applicable in this case; the long-range character of the potential generates only small corrections $\sim(\sigma/L)^2$. In the opposite case $L < \sigma$ we get a saturation of $\Gamma(L)$ for separated levels and the linear L dependence of the linewidth for the overlapped ones.

We evaluate also the damping of optical phonons in nanoparticles due to strong rare pointlike impurities. Investigating the regimes of separated and overlapped levels at arbitrary mass variation $|\delta m| \gtrsim m$ we obtain the same L dependencies of the linewidths as for the weakly disordered case, but the disorder strength dependence is more involved. The most interesting situations are the unitary limit for impurity scattering when the mass variation does not enter the formulas, and the regime of resonant scattering when we observe the parametric enhancement of the damping. The latter regime is connected with the problem of formation of the impurity-phonon bound state also investigated in the present paper.

Technically, our approach in paper I can be described as follows. In order to address the problem comprehensively, we successively evaluate the broadening of optical phonon spectral lines in nanoparticles due to the scattering (i) off weak pointlike Gaussian (Born) impurities and (ii) in the weak *smooth* random Gaussian potential, as well as (iii) due to the strong dilute binary disorder. When studying separated levels we apply the self-consistent Born approximation for the first two problems, the diagram technique being formulated in the basis of eigenfunctions of the problem. Strong impurities are treated within the T-matrix approximation for both cases. When investigating the overlapped levels we utilize the fact that the eigenfunctions are essentially

extended in this case. This allows us to replace them by plane waves thus formulating the ordinary bulk problem within the momentum representation and making the size quantization replacement of the momentum $q \to q_n(L, p)$ only in final formulas. For example, in cubic particles $p = 6$ and $q_n = (\pi/L)P_6\sqrt{n_x^2 + n_y^2 + n_z^2}$, where $n_{x,y,z}$ are the quantum numbers related to size quantization in the cubic box, with P_p being the factor converting the linear measure of a particle with faceting number p (e.g., the cube edge) into the diameter of a sphere which contains the same number of atoms, $P_6 = (\pi/6)^{-1/3}$.

In paper II we focus on the *numerical* studies of disorder-induced broadening of vibrational modes in nanoparticles. We use the atomistic DMM and the continuous EKFG models in order to obtain the phonon eigenfunctions and the corresponding eigenfrequencies. This allows us to implement the "model" Gaussian disorder for direct comparison with the analytics and to investigate Gaussian and binary disorder, smooth disorder, isotopic impurities, vacancies, and NV centers (nitrogen + vacancy) within the unified scheme. This scheme includes the numerical evaluation of the phonon Green's function for each state of a pure particle with their subsequent averaging over disorder realizations. The typical statistical sampling was no less than several hundred (to be precise, 128, 256, or 384 depending on the problem at hand). Also, we use the continuous EKFG model for the treatment of particle surface imperfections, for which case we introduce and investigate the models of "peeled apples" and "nibbled apples."

Some results of the present work have been reported in Ref. [40].

Paper I is organized as follows. Section II contains a short description of approaches of Refs. [26,27] necessary to make the understanding of the line broadening problem more clear and fluent. In Sec. III we introduce the Hamiltonian and sketch the Green's function formalism for dirty optical phonons in the situation when the energy levels are separated (overlapped). Then we calculate the spectral line broadening within the weak delta-correlated Gaussian impurity potential (pointlike Born impurities). In Sec. IV we extend our treatment to the case of weak and smooth random potential, while in Sec. V we elaborate the case of strong rare impurities, the latter being evaluated within the T-matrix method. Finally, Sec. VI summarizes our analytical results. The comparative discussion of separated and overlapped level broadening is also presented. An example of the application of our general approach (EKFG method for cubic particles) can be found in the Appendix.

II. BRIEF OVERVIEW OF DMM-BPM AND EKFG APPROACHES

This paper is devoted to the (analytical) treatment of the role of *disorder* in the problem of vibrational eigenmode broadening in nanoparticles, so no detailed knowledge is needed about the theory used to evaluate the "clean" spectra. Nevertheless, for the sake of integrity of presentation we supply it with a brief outline of two theoretical methods we advocate for spectral calculations. Their detailed description can be found in Refs. [26,27].

The program of interpretation of the Raman peak for a powder of particles of a given sort consists of four steps. The *first* one is the solution of the vibrational eigenproblem providing a set of phonon eigenfrequencies and eigenfunctions. In our first approach [26] this step is implemented with the use of the *dynamical matrix method* [41] which is a direct solution of the $3N \times 3N$ matrix equation of motion for mechanical vibrations:

$$m\,\omega^2 r_{l,\alpha} = \sum_{l'=1}^{N} \sum_{\beta=x,y,z} \frac{\partial^2 \Phi}{\partial r_{l,\alpha}\partial\, r_{l',\beta}} r_{l',\beta}, \tag{1}$$

where N is the number of atoms in a particle, $r_{l,\alpha}$ is the lth atom displacement along the direction α, m is the mass of the atom, ω is the frequency, and Φ is the total energy of a particle as a function of atomic displacements. The function Φ could be extracted from any mechanistic theory of crystals; we use the Keating model [42]. This straightforward approach has only one disadvantage: it takes quite a long time to evaluate numerically $3N \times 3N$ matrices, so the particles exceeding 6 nm ($\sim$20 000 atoms) are hardly analyzable on present-day PC clusters.

One of the ways to avoid this difficulty is realized in our second approach. It has been demonstrated in Ref. [27] that the long-wavelength limit of the discrete DMM problem Eq. (1) for optical phonon modes is governed by the continuous Klein-Fock-Gordon equation in the Euclidean space (EKFG) with the Dirichlet boundary conditions:

$$\left(\partial_t^2 + C_1\Delta + C_2\right)Y = 0, \quad Y|_{\partial\Omega} = 0. \tag{2}$$

Here $C_{1,2}$ are some positive constants which can be expressed via the parameters of a microscopic theory, Y are the eigenfunctions to be obtained in the course of solution of the problem, $\partial\,\Omega$ is the nanoparticle boundary. This latter equation is much easier to solve for an arbitrary particle shape even for the particle size essentially larger than 6 nm with the use of the routine Mathematica [43] apparatus.

The *second* step of calculations is the elaboration of spectral characteristics obtained at the first step in order to figure out how they manifest themselves in the optical experiment, i.e., as a result of certain photon-phonon interactions. For this aim we used the *bond polarization model* which is known to be appropriate for the description of the photon scattering in nonpolar crystals under the Raman experimental conditions [37]. In this model the polarization tensor $P_{\alpha\beta}$ for the nth phonon mode is given by

$$P_{\alpha\beta}(n) = \sum_{l=1}^{N} \sum_{\gamma} M_{l,\alpha,\beta,\gamma}\, r_{l,\gamma}(n), \tag{3}$$

with $M_{l,\alpha,\beta,\gamma}$ being some combinations of atomic radius vectors and material constants, which could be expressed via the microscopic parameters of the theory [26], as well.

Analyzing theoretically the spectral properties of diamond nanocrystals of various shapes, we observe a very helpful common feature of them, namely, existence of Raman "active" (strongly contributing) and "silent" (almost not contributing) modes in the spectrum. This allows us to formulate the approximate analytical version of the DMM-BPM [26] which is much easier to evaluate, thus making it applicable

for larger particles than the regular DMM-BPM allows. Furthermore, for the EKFG method we developed the continuous version of BPM, and the Raman intensity of the nth mode of a single particle with volume V now reads

$$I_n = \left| \int Y_n \, dV \right|^2. \tag{4}$$

This makes it possible to obtain the outcome of EKFG calculations with nearly the same accuracy as can be done with the use of the more direct DMM-BPM method.

As a result of these first two steps the Raman spectra are given by dense series of zero-width spectral lines with intrinsic structure peculiar to and characteristic of the shape and the sort of particles studied. The *third* step needed to describe the Raman experiment is to broaden these lines replacing zero-width delta functions by Lorentzians and thus introducing the damping of individual eigenmodes. This damping is known to be much larger for nanoparticles than for relevant bulk materials [44]. In our previous calculations, we treated the linewidth Γ as a fitting parameter. The present work is intended to certify the disorder as the main microscopic source of the phonon line broadening observed in Raman experiments and to express the fitting parameters via the microscopic characteristics of disordered nanocrystals.

After the spectral lines are properly broadened, we end up with the Raman peak (or peaks) as would exist for a powder of equal-sized particles. The *fourth* step of calculations is to include the size distribution function. The easiest way to do it is to apply for spectral lines the scaling arguments developed in [27] within the EKFG approach:

$$I_{L_2}(\omega) = \left(\frac{L_2}{L_1}\right)^3 I_{L_1}\left(\omega_0 - (\omega_0 - \omega)\left(\frac{L_2}{L_1}\right)^2\right). \tag{5}$$

Here $I_{L_{1,2}}(\omega)$ are the spectra of particles which both have the same shape but different sizes L_1 and L_2, respectively.

Empirically, the EKFG scaling Eq. (5) may be extended onto the DMM-BPM approach, as well, which can be justified by the similarity of spectra obtained with the use of both these methods. This allows us to incorporate the size distribution into the theory without boring recalculation of spectra for each particle size contained in the distribution function, as one should do at the first glance.

Notice that the Raman peaks calculated within the DMM-BPM and the EKFG methods look very similar. They also fit existing experimental data for small nanoparticles much better than the previous theories even with the empirical broadening procedure undertaken instead of the third step of the approach of this section (see [26,27] and Fig. 2).

III. WEAK POINTLIKE IMPURITIES

In this section we introduce a diagram technique for the disordered phonon problem and discuss the phonon scattering by Born impurities in two qualitatively different regimes of separated and overlapped energy levels.

A. General formalism

Let us start the derivation of the Hamiltonian of "dirty phonons" from the more general one,

$$\mathcal{H} = \sum_l \frac{p_l^2}{2m_l} + \frac{1}{2}\sum_{ll'} K_{ll'}(\mathbf{r}_l - \mathbf{r}_{l'})^2, \tag{6}$$

where the first sum runs over all the lattice sites l, and the atomic mass m_l varies from site to site. The second sum includes all pairs of atoms, with spring rigidities being $K_{ll'}$, and $\mathbf{r}_l$ stand for the corresponding displacements.

As we mentioned above the phonon line broadening problem in a nanoparticle should be treated separately depending on whether this broadening results in the level overlap or not. For weak enough disorder and/or for small enough particles we are definitely in the regime of separated levels. In order to describe this regime it is convenient to use the Green's function formalism formulated in the basis of eigenfunctions of a given problem.

In a particle containing N atoms there are $3N$ normalized to the unity vibrational modes $\mathbf{Y}_n(\mathbf{R}_l)$ with energies ω_n. Here n is the generalized (multicomponent) quantum number of our eigenproblem. Assuming all the masses to be equal to each other (as, e.g., in diamond) for atom displacements and momenta we have

$$\mathbf{r}_l = \frac{1}{\sqrt{2m}}\sum_n \frac{\mathbf{Y}_n(\mathbf{R}_l)}{\sqrt{\omega_n}}(b_n + b_n^\dagger) \tag{7}$$

and

$$\mathbf{p}_l = \frac{i\sqrt{m}}{\sqrt{2}}\sum_n \mathbf{Y}_n(\mathbf{R}_l)\sqrt{\omega_n}(b_n^\dagger - b_n), \tag{8}$$

respectively. Using Eqs. (7) and (8) one gets the Hamiltonian in the form $\mathcal{H} = \mathcal{H}_{ph} + \mathcal{H}_{\rm imp}$, where the first term yields the phonon energy

$$\mathcal{H}_{ph} = \sum_n \omega_n (b_n^\dagger b_n + 1/2). \tag{9}$$

The second term $\mathcal{H}_{\rm imp}$ specifies how the disorder affects vibrational modes. Hereinafter we shall assume for simplicity that the disorder appears in the problem via the mass variation only (another source of disorder would be random rigidities). For the simplest pointlike impurities the perturbation of the bare Hamiltonian $\mathcal{H}_{ph}$ reads

$$\mathcal{H}_{\rm imp} = \frac{1}{2}\sum_l \delta m_l^{-1} p_l^2, \tag{10}$$

with the inverse-mass variation δm_l^{-1} given by

$$\delta m_l^{-1} = \frac{1}{m + \delta m_l} - \frac{1}{m} \approx -\frac{\delta m_l}{m^2}, \tag{11}$$

where

$$m = \langle m_l \rangle, \tag{12}$$

and the random masses are supposed to be Gaussian delta-correlated quantities with zero averages

$$\left\langle \delta m_l^{-1} \right\rangle = 0, \quad \langle \delta m_l \rangle = 0, \tag{13}$$

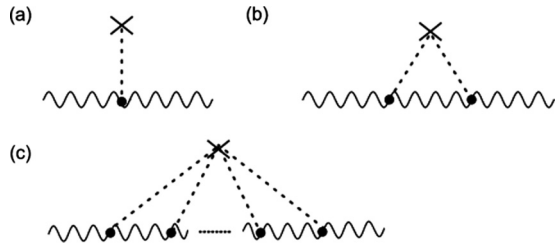

FIG. 4. Diagrams for the phonon scattering by disorder evaluated in the present paper. (a) A single scattering by the impurity does not lead to the phonon damping. (b) The diagram giving the leading contribution to the phonon self-energy in the Born regime. The self-consistent Born approximation appears when replacing the bare phonon propagator under the "impurity arch" by the full one. For strong rare impurities one should sum up all the diagrams of the type (c) taking into account multiple scattering by the same impurity (T-matrix approximation).

and delta-functional pairwise correlators

$$\langle \delta m_l \, \delta m_{l'} \rangle / m^2 \; = \; \delta_{ll'} \, c_{\rm imp} \left(\frac{\delta m}{m} \right)^2 \; \equiv \; \delta_{ll'} \, S. \tag{14}$$

Here $S \ll 1$ is the dimensionless strength of disorder. "Strong" impurities ($S \lesssim 1$) with nonzero average will be considered in Sec. V of this paper.

Using Eq. (8) we can write the impurity-induced perturbation in the form

$$\mathcal{H}_{\rm imp} = -\frac{m}{4} \sum_{l,n,n'} \mathbf{Y}_n(\mathbf{R}_l) \cdot \mathbf{Y}_{n'}(\mathbf{R}_l) \, \delta m_l^{-1} \sqrt{\omega_n \omega_{n'}} (b_n^\dagger - b_n)(b_{n'}^\dagger - b_{n'}). \tag{15}$$

Let us introduce the Green's function $-i\langle \hat{\mathrm{T}} \, \phi_n \phi_n \rangle$ for operators $\phi_n = i(b_n^\dagger - b_n)$, where $\hat{\mathrm{T}}$ stands for the time-ordering operator. Upon an averaging over impurity configurations, the self-energy $\Pi_n(\omega)$ arising due to the phonon scattering by disorder enters this Green's function in the following way:

$$D_n(\omega) = \frac{2\omega_n}{\omega^2 - \omega_n^2 - 2\omega_n \Pi_n(\omega)}. \tag{16}$$

To the leading order in the impurity strength S only the diagram shown in Fig. 4(b) contributes to the phonon self-energy [diagram Fig. 4(a) is zero due to condition Eq. (13)], and the corresponding contribution reads

$$\Pi_n(\omega) = \frac{S\omega_n}{16} \sum_{l,n'} [\mathbf{Y}_n(\mathbf{R}_l) \cdot \mathbf{Y}_{n'}(\mathbf{R}_l)]^2 \, \omega_{n'} D_{n'}(\omega). \tag{17}$$

This equation will be solved in the next subsection. When the disorder increases the levels start to overlap. Another way to obtain the overlapped states is to treat large particles. For both these situations it is convenient to use the ordinary (bulk) diagram technique in the momentum space and then incorporate the finite-size quantization $q \to q_n(L, p)$ in final formulas; the quantization rule $q_n(L, p)$ depends on the shape of a particle.

For bulk crystals one can use standard expressions for atomic displacements and momenta via the phonon creation-annihilation operators $b_{\mathbf{q}\nu}^\dagger$ ($b_{\mathbf{q}\nu}$):

$$\mathbf{r}_l = \frac{1}{\sqrt{2Nm}} \sum_{\mathbf{q}\nu} \frac{\mathbf{P}_\mathbf{q}}{\sqrt{\omega_{\mathbf{q}\nu}}} (b_{\mathbf{q}\nu}^\dagger e^{-i\mathbf{q}\mathbf{R}_l} + b_{\mathbf{q}\nu} e^{i\mathbf{q}\mathbf{R}_l}), \tag{18}$$

$$\mathbf{p}_l = \frac{i\sqrt{m}}{\sqrt{2N}} \sum_{\mathbf{q}\nu} \mathbf{P}_\mathbf{q} \sqrt{\omega_{\mathbf{q}\nu}} (b_{\mathbf{q}\nu}^\dagger e^{-i\mathbf{q}\mathbf{R}_l} - b_{\mathbf{q}\nu} e^{i\mathbf{q}\mathbf{R}_l}). \tag{19}$$

Here $\mathbf{P}_\mathbf{q}$ is the phonon polarization and the index ν runs over all branches of the optical spectrum. For longitudinal phonons $\mathbf{P}_\mathbf{q} = \mathbf{e}_\mathbf{q} = \mathbf{q}/q$, and for transverse ones $\mathbf{P}_\mathbf{q} \perp \mathbf{e}_\mathbf{q}$. Using Eqs. (18) and (19) we obtain the Hamiltonian $\mathcal{H}_{ph}$ in the form

$$\mathcal{H}_{ph} = \sum_{\mathbf{q}\nu} \omega_{\mathbf{q}\nu} (b_{\mathbf{q}\nu}^\dagger b_{\mathbf{q}\nu} + 1/2), \tag{20}$$

where $\omega_{\mathbf{q}\nu}$ is the bare phonon frequency. For the sake of simplicity, the phonon spectrum is taken to be identical in all branches; the generalization onto the case of different parameters is straightforward. We shall be interested in the optical phonons near the Brillouin zone center, where their dispersion is well approximated by the formula

$$\omega_\mathbf{q} = \omega_0 - \alpha q^2 = \omega_0 [1 - F(qa_0)^2]. \tag{21}$$

Here we introduce the dimensionless parameter of flatness of the optical phonon spectrum F:

$$F = \frac{1}{2\omega_0 a_0^2} \left(\frac{\partial^2 \omega_\mathbf{q}}{\partial q^2} \right)_{\mathbf{q}=0}, \tag{22}$$

and a_0 is the lattice parameter. Relations between phenomenological parameters ω_0 and α and the parameters of the microscopic Keating model [42] for materials under investigation can be found, for instance, in Refs. [26] and [27].

We can rewrite the interaction term Eq. (10) as follows:

$$\mathcal{H}_{\rm imp} = \frac{m}{4N} \sum_{l,\, \mathbf{q}_{1,2},\nu} (\mathbf{P}_{\mathbf{q}_1} \cdot \mathbf{P}_{\mathbf{q}_2}) \, \delta m_l^{-1} \sqrt{\omega_{\mathbf{q}_1\nu} \, \omega_{\mathbf{q}_2\nu}} \times \left[b_{\mathbf{q}_1\nu}^\dagger b_{\mathbf{q}_2\nu} e^{i(\mathbf{q}_2 - \mathbf{q}_1)\mathbf{R}_l} - b_{\mathbf{q}_1\nu} b_{\mathbf{q}_2\nu} e^{i(\mathbf{q}_2 + \mathbf{q}_1)\mathbf{R}_l} \right] + \text{H.c.}, \tag{23}$$

where H.c. stands for Hermitian conjugate. The diagram technique for the Hamiltonian Eqs. (20) and (23) (see, e.g., Ref. [45]) is very similar to the one widely used for disordered electrons (cf. Ref. [46]). The Green's function $D(\omega, \mathbf{q})$ is built upon the bosonic field operators $\phi(\mathbf{q}) \propto b_\mathbf{q} - b_{-\mathbf{q}}^\dagger$. The bare phonon propagator is given by

$$D_0(\omega, \mathbf{q}) = \frac{2\omega_\mathbf{q}}{\omega^2 - \omega_\mathbf{q}^2 + i0}. \tag{24}$$

After averaging over impurity configurations, the disorder-induced self-energy $\Pi_\mathbf{q}(\omega)$ enters this equation in the following way:

$$D^{-1}(\omega, \mathbf{q}) = D_0^{-1}(\omega, \mathbf{q}) - \Pi_\mathbf{q}(\omega). \tag{25}$$

To the leading order in S the analog of Eq. (17) reads

$$\Pi_\mathbf{q}(\omega) = \frac{S \, \omega_\mathbf{q}}{16N} \sum_\mathbf{k} \omega_\mathbf{k} D_0(\omega, \mathbf{k}), \tag{26}$$

where the proper choice of coordinates allowed us to eliminate the contribution from one of the phonon branches.

It should be mentioned the similarity between our formulas for separated and overlapped levels; cf. Eqs. (16) and (25) as well as Eqs. (17) and (26). However, the final results for these two cases are drastically different.

B. Separated levels

When using the formal perturbation theory in the parameter S the phonon self-energy on the right-hand side of Eq. (17) should be omitted. It can be shown that no broadening of the phonon line appears in this case. We shall use the self-consistent Born approximation keeping the self-energy on the right-hand side of Eq. (17) finite, and thus obtaining $\Pi_n(\omega)$ self-consistently. This method resembles an approach used for disorder-induced broadening of Landau levels in a two-dimensional degenerate electron gas subject to high magnetic fields [47]. Following the same line we consider an equation

$$\Pi_n(\omega) = \frac{S\omega_n}{8} \sum_{l,n'} \frac{[\mathbf{Y}_n(\mathbf{R}_l) \cdot \mathbf{Y}_{n'}(\mathbf{R}_l)]^2 \, \omega_{n'}^2}{\omega^2 - \omega_{n'}^2 - 2\omega_{n'}\Pi_{n'}(\omega)}. \tag{27}$$

One can easily see that for nonoverlapped levels this equation contains effectively only the term with $n' = n$. For nondegenerate levels it yields

$$\Pi_n(\omega) = \frac{2\, c_n^2(p)\, S\, \omega_n^3}{N} \frac{1}{\omega^2 - \omega_n^2 - 2\omega_n \Pi_n(\omega)}. \tag{28}$$

Here $c_n^2(p) = N \sum_l [\mathbf{Y}_n(\mathbf{R}_l)]^4/16$ is a certain shape p and quantum number n dependent coefficient. Solving Eq. (28) we obtain

$$\Pi_n(\omega) = \frac{\omega^2 - \omega_n^2 - \sqrt{(\omega^2 - \omega_n^2)^2 - \dfrac{16 c_n^2(p) S \omega_n^4}{N}}}{4\omega_n}. \tag{29}$$

When the square root in Eq. (29) is imaginary it determines the phonon damping which leads to the well-known semicircle law for the density of states [47]. Similarly to the case of disordered electrons in high magnetic fields, the range of validity for this self-consistent solution is limited by the proximities of semicircle maxima, whereas near their edges one should take into account the phonon scattering by rare configurations of impurities which results in exponential tails in the density of states (see Ref. [48] and references therein). However, if we are not interested in these details, one can use the crude Lorentzian (on-shell) approximation. This approximation ($\omega = \omega_n$) in Eq. (29) leads to the phonon damping in the form

$$\Gamma_n = \omega_n \, c_n(p) \sqrt{\frac{S}{N}}. \tag{30}$$

The definition of Γ we use in papers I and II differs from that of Refs. [26,27,40] where the width of the Lorentzian has been parameterized by $\Gamma/2$ rather than Γ of the present work.

The semicircle shape of a spectral line in the independent-levels approximation and its simplified Lorentzian form are shown in Fig. 5.

Next, we express the number of atoms N in a particle via its effective size L. (For example, cubic particles provide $N \to (2L\,/\,P_6\, a_0)^3$, the lattice assumed to be cubic with two atoms in the unit cell.) This finally yields

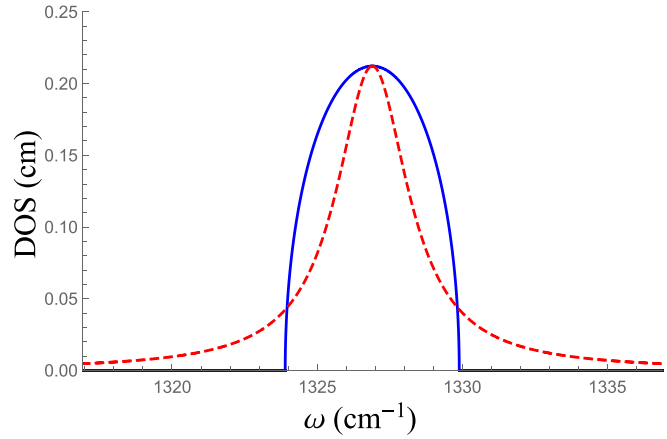

FIG. 5. The shape of a spectral line in the regime of separated levels (blue line) has a symmetric semicircle form. Its on-shell approximation leads to the standard Lorentzian shape (red dashed curve).

$$\Gamma_n = \omega_n \, \mu_n(p) \sqrt{S} \left(\frac{a_0}{L}\right)^{3/2}. \tag{31}$$

Here we absorbed the shape-dependent parameter P_p into $\mu_n(p) = c_n(p)\sqrt{P_p^3/8}$. The constant $\mu_n(p)$ can be calculated analytically for cubic, spherical, and cylindrical particles and numerically for any other shape of particles.

The real correction to the phonon self-energy stemming from other energy levels can be found from Eq. (27) without self-consistency:

$$\Pi_n(\omega) = \frac{S\omega_n}{8} \sum_{l,n' \neq n} \frac{[\mathbf{Y}_n(\mathbf{R}_l) \cdot \mathbf{Y}_{n'}(\mathbf{R}_l)]^2 \omega_{n'}^2}{\omega^2 - \omega_{n'}^2}. \tag{32}$$

This weakly ω-dependent correction originates from the many phonon modes in the spectrum and results mainly in the effective renormalization of ω_0 for the highest (i.e., closest to the Brillouin zone center) modes.

C. Overlapped levels

The difference between separated and overlapped levels is evident already when comparing Eq. (17) and Eq. (26). First, the sum over n' in Eq. (17) could be safely omitted within the independent-levels approximation while the integration over intermediate momenta in Eq. (26) is an essential ingredient of the theory. Second, the nonzero linewidth for separated levels appears only due to the *self-consistent* treatment while in the continuum the phonon line broadening is provided by the regular perturbation theory in S. In the latter case one gets

$$\mathrm{Im}\, \Pi_{\mathbf{q}}(\omega) = -\frac{\pi S \omega_{\mathbf{q}}}{16N} \sum_{\mathbf{k}} \omega_{\mathbf{k}} [\delta(\omega + \omega_{\mathbf{k}}) + \delta(\omega - \omega_{\mathbf{k}})]. \tag{33}$$

Equation (33) contains two delta functions. Since we are interested in its behavior in the vicinity of the positive pole $\omega \approx \omega_{\mathbf{q}}$ of the Green's function, the phonon dispersion does not allow

the argument of the delta function $\delta(\omega+\omega_{\mathbf{k}})$ to reach zero value anywhere in the Brillouin zone, so this term gives zero contribution to the integral. Hence, the only delta function which contributes is $\delta(\omega-\omega_{\mathbf{k}})$. Notice that in the vicinity of the negative pole $\omega\approx-\omega_{\mathbf{q}}$ the situation is opposite. Then using the expansion of the optical phonon spectrum near its maximum, one obtains

$$\mathrm{Im}\,\Pi_{\mathbf{q}}(\omega)=-\frac{S\,a_0^3\,\omega_{\mathbf{q}}}{64\,\pi\,\alpha^{3/2}}\,\theta(\omega_0-\omega)\,\omega\,\sqrt{\omega_0-\omega}. \tag{34}$$

We see that the imaginary part of $\Pi_{\mathbf{q}}(\omega)$ is nonzero only for frequencies lower than ω_0. Moreover, it reveals a square-root nonanalytical behavior when $\omega\to\omega_0$ originated from the van Hove singularity in the phonon density of states that occurs at this energy.

The real part of $\Pi_{\mathbf{q}}(\omega)$ can be calculated in a similar manner, and the result is given by

$$\mathrm{Re}\,\Pi_{\mathbf{q}}(\omega)=-\frac{S\,a_0^3\,\omega_{\mathbf{q}}}{64\,\pi\,\alpha^{3/2}}\,\theta(\omega-\omega_0)\,\omega\,\sqrt{\omega-\omega_0}. \tag{35}$$

This result is essentially frequency-dependent in the vicinity of the phonon pole $\omega\simeq\omega_{\mathbf{q}}\approx\omega_0-\alpha q^2$. Likewise Eq. (34) it stems from the van Hove singularity in the spectra of intermediate phonons scattered by disorder. It can be evaluated either directly or from the imaginary part of $\Pi_{\mathbf{q}}(\omega)$ via the Kramers-Kronig relations; see [46,49].

In addition to Eq. (35), there appears one more term which is almost constant near the pole $\omega\approx\omega_{\mathbf{q}}$ and proportional to the Debye momentum q_D that comes from the upper limit of the integration over the Brillouin zone in Eq. (26). It is the momentum domain wherein the details of the phonon band structure become important, and the Debye approximation is valid only qualitatively. Moreover, the Keating model we use in our calculations essentially fails in this area. This makes the numerical prefactor in front of the high-momenta contribution very unreliable. Also, similar contributions stem in this case from both $(\omega\pm\omega_{\mathbf{k}})^{-1}$ poles of the integrand in Eq. (26). In fact, this term has the same origin as the contribution discussed below for certain types of disorder with nonzero mean value $\langle\delta m_l^{-1}\rangle$ which provides the constant shift of the real part of the phonon self-energy. Below we shall concentrate on a strongly frequency- and momentum-dependent part of the self-energy assuming that all constant ($\mathbf{q}$, ω-independent) terms are already absorbed into ω_0 (see, however, Sec. V and paper II).

Notice that the real and the imaginary parts of $\Pi_{\mathbf{q}}(\omega)$ can be conveniently rewritten jointly as follows:

$$\Pi_{\mathbf{q}}(\omega)=-\frac{S\,a_0^3\,\omega_{\mathbf{q}}}{64\,\pi\,\alpha^{3/2}}\,\omega\,\sqrt{\omega-\omega_0}. \tag{36}$$

Substituting Eq. (36) into Eq. (25) we can draw the spectral weight of the phonon Green's function

$$A_{\mathbf{q}}(\omega)=-\frac{1}{\pi}\mathrm{Im}D_{\mathbf{q}}(\omega). \tag{37}$$

This function, depicted in Fig. 6 (blue curve), represents the broadened spectral line of the optical phonon (rigorously speaking, in the bulk). Our first observation is that the shape of the line is quite asymmetric. This asymmetry originates from the nontrivial frequency dependence of both the real and the imaginary parts of the self-energy which take place in different frequency domains. It is the common feature in many physical problems where the self-energy demonstrates visible frequency variation near the quasiparticle pole (see, e.g., Ref. [50]). Let us perform, however, the *on-shell approximation*:

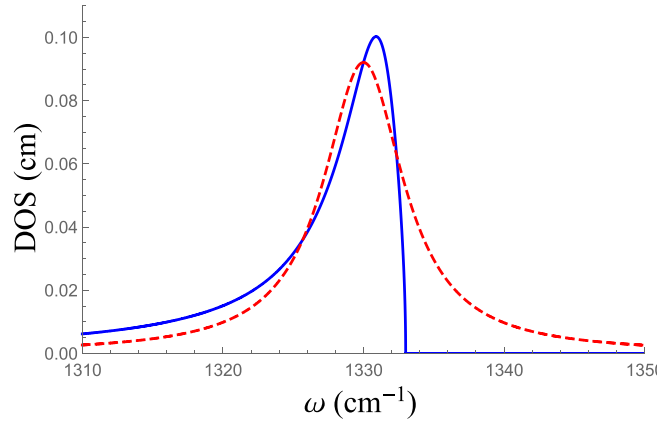

FIG. 6. The shape of a spectral line in the regime of overlapped levels (blue curve). The spectral weight is essentially asymmetric. Conventional Lorentzian shape (red dashed curve) can be obtained using the on-shell approximation.

$$\Gamma_{\mathbf{q}}(\omega)=-\frac{2\omega_{\mathbf{q}}\mathrm{Im}\Pi_{\mathbf{q}}(\omega)}{\omega+\omega_{\mathbf{q}}}\to\Gamma_{\mathbf{q}}(\omega=\omega_{\mathbf{q}})\equiv\Gamma_{\mathbf{q}}. \tag{38}$$

Making this substitution in Eq. (37) we observe that the resulting curve becomes Lorentzian (see Fig. 6, red dashed line), i.e., symmetric near its maximum, the width of the peak being close to the real one *as far as the interaction-induced effects are small*.

Ignoring the line-shape asymmetry yields the phonon linewidth in the form

$$\Gamma_{\mathbf{q}}=\omega_{\mathbf{q}}^2\,\frac{S\,a_0^3}{64\pi\,\alpha}\,q=\omega_{\mathbf{q}}\,\frac{S}{64\pi F}\,(q\,a_0). \tag{39}$$

The linear-in-q dependence of the broadening parameter $\Gamma_{\mathbf{q}}$ here is very important. Until now our consideration was related to the bulk phonon-impurity model. Now we perform the finite-size quantization $q\to q_n(L,p)$ in Eq. (39). It immediately yields the linewidth dependence on the particle size in the desirable [38] $1/L$ form:

$$\Gamma_n=\omega_n\,\nu_n(p)\,S\,\frac{a_0}{L}. \tag{40}$$

Here $\nu_n(p)$ is the shape-dependent coefficient which contains (i) the numerical prefactor $1/64$, (ii) the spectrum flatness parameter F in denominator, and (iii) the strong dependence on the quantum number n. From the above consideration it follows that the phonon modes with large n are broadened stronger than the first one. In particular, for cubic particles their widths are related to each other as

$$\Gamma_{n_x,n_y,n_z}=\sqrt{\frac{n_x^2+n_y^2+n_z^2}{3}}\,\Gamma_1. \tag{41}$$

Notice that for Raman-active modes all quantum numbers n_i must be odd in this case (see Eqs. (4) and (A12); for the detailed discussion of this issue see also Ref. [26]).

Above we investigated how weak disorder affects the phonon linewidth. For separated levels we observed a semicircle law for the phonon DOS and $\Gamma \propto \sqrt{S}/L^{3/2}$ behavior of the linewidth; the prefactor is some weakly shape and quantum number dependent quantity. For overlapped levels we found that the phonon line shape is asymmetric due to the van Hove singularity in the spectrum. Within the on-shell approximation we obtained that the damping is proportional to S/L with the prefactor strongly dependent on the phonon quantum number.

IV. SMOOTH RANDOM POTENTIAL

Section III has been devoted to the treatment of the weak pointlike (delta-correlated) Gaussian disorder. Now we shall consider how a smooth character of the (still, weak) random impurity potential affects the results of the previous section. More specifically, instead of the pointlike impurities of Eq. (14) we shall assume the long-range character of the impurity-impurity correlation function

$$\begin{aligned}\left\langle \delta m_l^{-1}\, \delta m_{l'}^{-1}\right\rangle m^2 &= \langle \delta m_l\, \delta m_{l'}\rangle m^{-2} \\ &= S\, W(|\mathbf{R}_l - \mathbf{R}_{l'}|;\sigma), \end{aligned} \tag{42}$$

where the characteristic scale σ of the potential is much longer than the lattice parameter, $\sigma \gg a_0$, and the correlation function is Gaussian:

$$W(r;\sigma) = \frac{a_0^3}{(2\pi\sigma^2)^{3/2}}\, \exp\left(-\frac{r^2}{2\sigma^2}\right), \tag{43}$$

where the prefactor is introduced for proper normalization.

Notice that the specific spatial dependence of the correlator in Eq. (42) is not essential; the only property needed is its rapid decay on the scale σ. For instance, we observe that replacing the Gaussian correlator in Eq. (43) by the exponential one does not change qualitatively our results.

A. Separated levels

Here we present our results for separated levels. We obtain the self-consistent equation for the phonon self-energy in the following form:

$$\begin{aligned}\Pi_n(\omega) = \frac{S\,\omega_n}{8} \sum_{l,l',n'} (\mathbf{Y}_{nl}\cdot\mathbf{Y}_{n'l'})\, W_{ll'}(\sigma)\, (\mathbf{Y}_{nl'}\cdot\mathbf{Y}_{n'l'}) \\ \times \frac{\omega_{n'}^2}{\omega^2 - \omega_{n'}^2 - 2\omega_{n'}\Pi_{n'}(\omega)}, \end{aligned} \tag{44}$$

where we used the shorthand notations $\mathbf{Y}_{nl} = \mathbf{Y}_n(\mathbf{R}_l)$ and $W_{ll'}(\sigma) = W(|\mathbf{R}_l - \mathbf{R}_{l'}|;\sigma)$. For nondegenerate phonon levels this yields

$$\Pi_n(\omega) = \frac{2\, d_n^2(p)\, S\, \omega_n^3}{N} \frac{1}{\omega^2 - \omega_n^2 - 2\omega_n\Pi_n(\omega)}, \tag{45}$$

where the parameter $d_n(p)$ is given by

$$d_n^2(p) = \frac{N}{16} \sum_{l,l'} \mathbf{Y}_{nl}^2\, W_{ll'}(\sigma)\, \mathbf{Y}_{nl'}^2. \tag{46}$$

These constants could be calculated for any particular model and particle shape. Up to the new prefactor $[d_n(p)$ instead of $c_n(p)]$ all the results of Sec. III B are applicable for the case of a smooth random potential. Once again, using the on-shell approximation we obtain the line broadening in the form

$$\Gamma_n = \omega_n\, \rho_n(p)\, \sqrt{S}\left(\frac{a_0}{L}\right)^{3/2}, \tag{47}$$

where $\rho_n(p)$ is the novel shape and quantum number dependent parameter, $\rho_n(p) = d_n(p)\sqrt{P_p^3/8}$.

The smooth character of disorder leads to the diminishing of the parameter $\rho_n(p)$ in comparison with $\mu_n(p)$ (see Appendix). Two regimes should be distinguished. The first one could be analyzed via an expansion in the small parameter $q_n\sigma \ll 1$, where $q_n(L, p)$ is the quantized discrete momentum, $\omega_n = \omega_0 - \alpha q_n^2$. The leading order contribution coincides with the result for pointlike impurities, the first correction being of the order of $(q_n\sigma)^2$.

The second regime that occurs at $q_n\sigma \gg 1$ appears exclusively due to the smoothness of the random potential. In this regime the wave functions in Eq. (46) experience fast oscillations on the scale σ and therefore could be replaced by their average values $\sim 1/\sqrt{N}$. As a result, the linewidth as a function of particle size L saturates:

$$\Gamma_n = \omega_n\, \frac{1}{4(2\pi)^{3/4}}\, \sqrt{S}\left(\frac{a_0}{\sigma}\right)^{3/2}. \tag{48}$$

The damping in this regime is small compared to the delta-correlated case (cf. Sec. III B).

B. Overlapped levels

The leading contribution to $\mathrm{Im}\,\Pi_{\mathbf{k}}(\omega)$ is determined by the same diagram Fig. 4 as for delta-correlated impurities. The corresponding analytical expression reads

$$\mathrm{Im}\,\Pi_{\mathbf{q}}(\omega) = -\frac{\pi S\omega_{\mathbf{q}}}{16N} \sum_{\mathbf{k}} \omega_{\mathbf{k}} \widetilde{W}(\mathbf{k}-\mathbf{q};\sigma)\delta(\omega - \omega_{\mathbf{k}}), \tag{49}$$

where $\widetilde{W}(\mathbf{q};\sigma)$ is the Fourier transform of Eq. (43):

$$\widetilde{W}(\mathbf{q};\sigma) = \exp\left(-\frac{q^2\sigma^2}{2}\right). \tag{50}$$

Integrating in Eq. (49) one obtains

$$\begin{aligned}\Gamma_{\mathbf{q}}(\omega) = -\frac{S\, a_0^3\, \omega_{\mathbf{q}}\, \omega}{64\,\pi}\, \frac{\theta(\omega_0 - \omega)}{2\,\alpha\,\sigma^2\, q} \\ \times \left\{ \exp\left[-\frac{1}{2}\frac{\sigma^2}{\alpha}(\sqrt{\alpha}q - \sqrt{\omega_0 - \omega})^2\right] \right. \\ \left. - \exp\left[-\frac{1}{2}\frac{\sigma^2}{\alpha}(\sqrt{\alpha}q + \sqrt{\omega_0 - \omega})^2\right]\right\}. \end{aligned} \tag{51}$$

The next step is to apply for Eq. (51) the on-shell approximation $\omega = \omega_{\mathbf{q}}$. This yields

$$\Gamma_{\mathbf{q}} = \Gamma_{\mathbf{q}}^0\, f(q\sigma), \tag{52}$$

where $\Gamma_{\mathbf{q}}^0$ is the bulk phonon damping for delta-correlated disorder [see Eq. (39)], and the spreading function $f(x)$ is

given by the following expression:

$$f(x) = \frac{1 - \exp[-2x^2]}{2x^2}. \tag{53}$$

Now we are ready to apply the finite-size quantization replacement $q \to q_n(L, p)$ in Eqs. (52) and (53),

$$\Gamma_n = \Gamma_n^0 f(q_n\sigma), \tag{54}$$

where Γ_n^0 is given by Eq. (40). This equation determines the damping of overlapped vibrational eigenmodes in finite nanoparticles subjected to the smooth random potential for arbitrary relation between L and σ.

It is instructive to investigate Eq. (54) in the limiting cases of small $q_n\sigma \ll 1$ and large $q_n\sigma \gg 1$ discrete momenta. The first asymptote yields $f(x) \to 1$ and therefore $\Gamma \approx \Gamma^0$; to the leading order the scale σ drops down from the formula. Thus, the damping function for the smooth disorder qualitatively reproduces its behavior peculiar for pointlike impurities. We conclude that for a finite nanoparticle which is essentially inhomogeneous on the scale of its size, $L \gtrsim \sigma$, the model of pointlike impurities qualitatively describes the case of smooth disorder, as well, and the resulting linewidth still mainly follows the $\Gamma \propto 1/L$ law.

However, when the discrete momentum is large, $q_n\sigma \gtrsim 1$, then $f(x) \approx 1/(2x^2)$, and the asymptotic behavior of damping in the smooth disorder described by Eq. (54) becomes $\Gamma_n \propto 1/q_n\sigma^2$ thus being drastically different from the Born case. In terms of finite-size particles this means that the long-range character of spatial variations of disorder manifests itself only when it occurs on scales of the order of or longer than the particle size, $\sigma \gtrsim L$, when the novel regime $\Gamma \propto L$ emerges:

$$\Gamma_n = \frac{\omega_n}{2}\left(\frac{1}{64\pi F}\right)^2\left(\frac{a_0}{\sigma}\right)^2 \nu_n^{-1}(p) S \frac{L}{a_0}. \tag{55}$$

Physically, the two regimes of momentum dependence for $\Gamma_{\mathbf{q}}$ could be understood from the general scattering theory [51] after we recognize that the particle velocity $\mathbf{v_q} \propto \nabla_{\mathbf{q}}\omega_{\mathbf{q}}$ is proportional to its momentum q. Then the first regime corresponds to the scattering of "slow" particles and the second one describes "fast" particles scattered by soft-core spheres with radii σ (see the problems in Ref. [51]).

Thus, when the particle size L is larger than the impurity length scale σ, i.e., when the nanoparticle is essentially inhomogeneous, the damping reveals the ordinary dependencies $1/L^{3/2}$ for separated and $1/L$ for overlapped phonon levels. Otherwise, the damping behavior changes to saturation for separated levels and to the linear-in-L dependence for overlapped levels; both crossovers occur when $L \sim \sigma$ (to be precise, the numerical factor 2π entering expansions moves crossovers toward larger L/σ values; see Fig. 7).

V. STRONG IMPURITIES

In this section we investigate the influence of strong rare impurities on the spectrum of optical vibrations in particles. We utilize the standard T-matrix approach (see, e.g, Ref. [52]) which treats exactly the multiple scattering events off a single impurity; see Fig. 4(c). It gives the correct result to the first order in $c_{\text{imp}} \ll 1$. A possibility to form the phonon-impurity bound state is also analyzed.

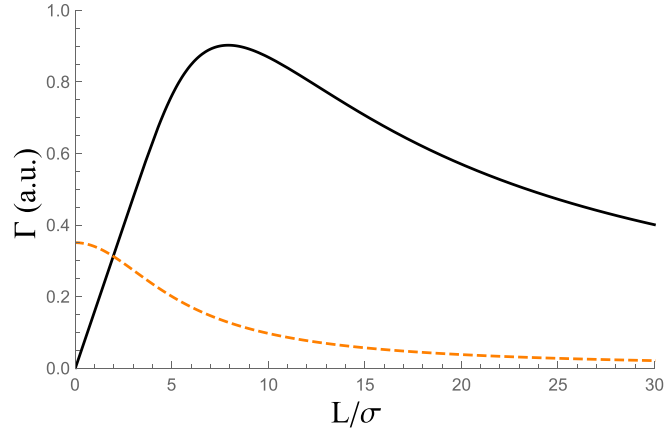

FIG. 7. Sketch of the phonon linewidth dependence on the particle size L, with σ being the characteristic length scale of the smooth random potential. Black line depicts the damping of the first phonon eigenmode [$q_1 \approx 2\pi/L$ in Eq. (54)] in the regime of overlapped levels. At small L the damping behaves as $\Gamma \propto L$, while for large L one observes the dependence peculiar for pointlike impurities, $\Gamma \propto 1/L$. In the regime of separated levels (orange dashed curve) the damping monotonically decreases from the finite value at small L toward zero as $\Gamma \propto 1/L^{3/2}$ when L increases.

More specifically, instead of the weak (Born Gaussian distributed) impurities with $(\delta m/m)^2 \ll 1$ and zero average $\langle \delta m_l \rangle = 0$ we introduce the binary distributed strong disorder (arbitrary $\delta m \gtrsim -m$). The mass variation reads

$$\delta m_l = \sum_{l'} \delta_{ll'}\, \delta m, \tag{56}$$

where the sum runs over all the impurity atoms located at sites l'; the masses of host atoms and impurity atoms are given by m and $m + \delta m$, respectively.

We also introduce the dimensionless impurity potential

$$U = \frac{\delta m}{m + \delta m}, \tag{57}$$

which will be useful for calculations below.

A. Separated levels

The T-matrix approximation presumes an exact solution of the single-impurity problem with its subsequent averaging over disorder configurations; the problem should be solved self-consistently. Let us discuss the first step. The contribution to $\Pi_n(\omega)$ stemming from all multiple scatterings off the impurity located at the lth site reads

$$\begin{aligned}\Pi_n^l(\omega) = \omega_n \sum_{k=1}^{\infty} \sum_{n_1,\ldots,n_{k-1}} \left(-\frac{U}{4}\right)^k (\mathbf{Y}_{nl} \cdot \mathbf{Y}_{n_1 l}) \\ \times (\mathbf{Y}_{n_1 l} \cdot \mathbf{Y}_{n_2 l}) \ldots (\mathbf{Y}_{n_{k-1} l} \cdot \mathbf{Y}_{nl}) \\ \times \omega_{n_1} D_{n_1}(\omega) \ldots \omega_{n_{k-1}} D_{n_{k-1}}(\omega);\end{aligned} \tag{58}$$

the kth term corresponds to the k-fold scattering off this impurity. As the next step, one should sum up the right-hand side of Eq. (58) over all impurity positions.

The independent-levels approximation allows us to solve this problem by putting all n_i in Eq. (58) equal to n. The

simple argument $|\mathbf{Y}(\mathbf{R})| \sim 1/\sqrt{N}$ allows us to estimate the kth contribution to Eq. (58) as $1/N^k$. Thus, at $|U| \sim 1$ it is sufficient to restrict our consideration by two first terms in Eq. (58) corresponding to diagrams (a) and (b) in Fig. 4. The first one is the (size-independent) rescaling of the phonon frequency ω_n due to the disorder-induced change of the average mass of atoms (cf. paper II):

$$\Pi_n^{(1)} = -\tfrac{1}{4}\,\omega_n\, U\, c_{\rm imp}. \tag{59}$$

The second term in Eq. (58) results in the self-consistent equation for $\Pi_n(\omega)$ which is equivalent to Eq. (28) where S should by replaced by $c_{\rm imp}\,U^2$. The counterpart of Eq. (31) reads

$$\Gamma_n = \omega_0\,\mu_n(p)\sqrt{c_{\rm imp}}|U|\Big(\frac{a_0}{L}\Big)^{3/2}. \tag{60}$$

Addressing the problem of localization of optical phonons by the impurities we notice that for $\delta m < 0$ this localization can appear at high frequencies $\omega > \omega_0$ because lighter atoms have higher vibrational eigenfrequencies. The corresponding analysis taking into account all phonon modes n_i in Eq. (58) and summing up all contributions of different orders in k can be realized for any particular set of model wave functions $\mathbf{Y}_n$ numerically but is hardly representable in general terms analytically. Moreover, the capability of an impurity to localize a phonon turns out to be strongly dependent on its location in a particle (see paper II). Therefore, we postpone the detailed discussion of localization issues to the next subsection where the boundary-induced phenomena are excluded from the consideration due to the "bulk" approach we use and to the paper II where they are addressed numerically in the most general form.

B. Overlapped levels

In the bulk all the contributions shown in Fig. 4(c) can be easily summed up as a geometric progression. After the averaging over disorder the phonon self-energy acquires the following standard form:

$$\Pi_{\mathbf{q}}(\omega) = -\frac{1}{4}\,\omega_{\mathbf{q}}\,\frac{c_{\rm imp}\,U}{1+\dfrac{U}{4N}\displaystyle\sum_{\mathbf{k}}\omega_{\mathbf{k}}\,D_0(\omega,\mathbf{k})}. \tag{61}$$

It is worth mentioning that $\Pi_{\mathbf{q}}(\omega)$ in Eq. (61) remains finite even for infinitely strong U ("unitary limit").

The integration in Eq. (61) is performed similarly to the Born case. One important difference comes from the fact that due to the different model of disorder (binary disorder with nonzero average) now we cannot absorb the constant term into ω_0. As a result we get

$$\frac{1}{N}\sum_{\mathbf{k}}\omega_{\mathbf{k}}\,D_0(\omega,\mathbf{k}) = \frac{\omega_0}{4\pi\alpha}\left[\frac{q_D}{\pi/2} - \sqrt{\frac{\omega-\omega_0}{\alpha}}\right], \tag{62}$$

where q_D is the Debye momentum (upper limit of integration). The quantity q_D is in fact a sort of adjustable parameter since its definition presumes that the spherical symmetry of the long-wavelength phonon spectrum could be extended onto large momenta. Therefore, the factor $\pi/2$ in Eq. (62) could not be treated seriously, and we just absorb it into the definition of Debye momentum using $q_D' = q_D/(\pi/2)$ instead of q_D.

Plugging Eq. (62) into Eq. (61), at $\omega < \omega_0$ we obtain

$$\Pi_{\mathbf{q}}(\omega) = -\,\omega_{\mathbf{q}}\,4\pi F^2\,\frac{c_{\rm imp}\,\omega_0}{\omega_{loc}-\omega}\left[\frac{a_0}{\zeta} + i\sqrt{\frac{\omega_0-\omega}{F\omega_0}}\right], \tag{63}$$

where the resonant frequency ω_{loc} (the binding energy of the phonon-impurity localized state; see below) is determined as follows:

$$\omega_{loc} = \omega_0 + \alpha\zeta^{-2}, \tag{64}$$

and the characteristic length ζ is given by

$$\zeta^{-1} = q_D'\left(1+\frac{16\pi F}{U q_D' a_0}\right). \tag{65}$$

This length is of the order of $1/q_D' \sim a_0$ for regular U and infinitely increases when $U \to U_{\rm min} = -16\pi F/q_D' a_0$. At $\omega > \omega_0$ we get $\mathrm{Im}\,\Pi_{\mathbf{q}}(\omega) = 0$; i.e., the damping is absent.

Consider the on-shell approximation $\omega = \omega_{\mathbf{q}}$. The damping acquires the form

$$\Gamma_{\mathbf{q}} = \omega_{\mathbf{q}}\,4\pi F\,c_{\rm imp}\left(\frac{\zeta}{a_0}\right)\frac{q\zeta}{1+(q\zeta)^2}. \tag{66}$$

After applying the finite-size quantization replacement $q \to q_n(L,p)$ this yields

$$\Gamma_n = \omega_n\,4\pi F\,c_{\rm imp}\left(\frac{\zeta}{a_0}\right)\frac{q_n\zeta}{1+(q_n\zeta)^2}. \tag{67}$$

We see that the behavior of the linewidth depends on the parameter ζ. When the spatial scale generated by this quantity is short, $\zeta \sim a_0$, the linewidth reveals the conventional $1/L$ behavior. If, however, ζ is a sort of critical quantity (this happens when $U \approx U_{\rm min}$), then it generates the long scale to be compared with L. For large $L \gg \zeta$ Eq. (67) yields $1/L$ particle size dependence with the additional enhancement factor $(\zeta/a_0)^2$. In the opposite case $L \ll \zeta$ the size dependence in Eq. (67) changes to linear-in-L; the situation resembles the crossover observed for the smooth random potential in Sec. IV.

Let us present the formula for the phonon linewidth in the unitary limit $U \to -\infty$ (or $\delta m \approx -m$, very light atoms or vacancies):

$$\Gamma_n = \omega_n\left(\frac{32F}{a_0 q_D}\right)^2 c_{\rm imp}\,\nu_n(p)\,\frac{a_0}{L}, \tag{68}$$

the strength of disorder does not enter this result. In contrast, for large positive $\delta m \gg m$ (very heavy impurities) disorder potential saturates at $U \to 1$ and there is no unitary limit.

In Fig. 8 we plot the linewidth dependence on the potential U for the first phonon mode in spherical 3 nm nanodiamonds. One can see the quadratic U dependence at $|U| \ll 1$ which corresponds to weak pointlike impurities (see Sec. III C), the resonant scattering when U is close to $U_{\rm min} \approx -0.2$, and the unitary limit at $U \lesssim -1$, when the damping is almost constant.

Importantly, Eq. (62) allows us to study a possibility to form the phonon-impurity bound state by investigating zeros of the denominator in Eq. (61) which determines the resonant energies of these states. At $\delta m > 0$ the localized states with

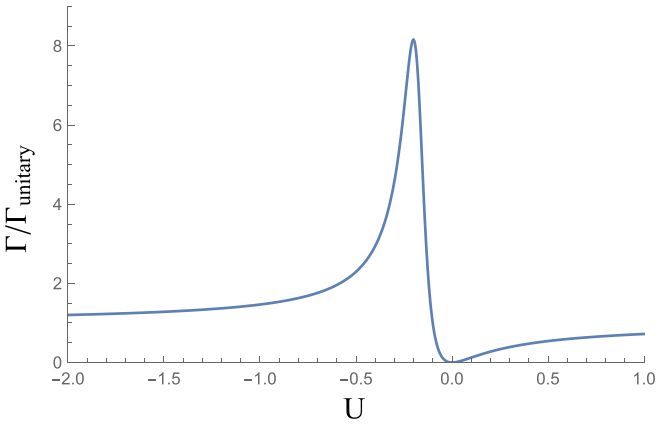

FIG. 8. Plot of the first phonon mode linewidth dependence on the disorder potential U in the regime of overlapped levels for spherical 3 nm nanodiamonds. We normalize the damping to its unitary limit which corresponds to $U \to -\infty$ or $\delta m \approx -m$ (very light impurities or vacancies). At small U the linewidth is proportional to U^2 as in the case of weak pointlike impurities. At negative U near the threshold of appearance of the isolated level $U_{\min} \approx -0.2$ the damping dramatically increases due to the resonant scattering. For phonons with higher momenta the resonance is much smoother.

$\omega > \omega_0$ do not appear because the denominator is positive in this frequency domain. Significant perturbations in the density of states may only be observed at frequencies corresponding to short-wavelength optical phonons or even below the optical band. These states are useless for the analysis of Raman spectra.

In the meantime, for light impurities with $\delta m < 0$ the situation is very different. At $U \leqslant U_{\min}$ the equation

$$1 + \frac{U a_0}{16\pi F}\left(q_D' - \sqrt{\frac{\omega - \omega_0}{\alpha}}\right) = 0 \tag{69}$$

has a solution given by Eq. (64). When $U \approx U_{\min}$, the frequency of localized level ω_{loc} is close to ω_0 and the phonon damping is drastically enhanced due to the resonant character of scattering off impurities. With the further decreasing of U toward unitarity the main contribution to the integral in Eq. (61) comes from the momenta lying beyond the range of applicability of the spectral expansion (21) and Eq. (62) fails. Here we just mention that in the improved theory $\omega_{loc} \propto |U|^{1/2}$.

We investigated the phonon damping due to strong dilute pointlike impurities. For separated levels we observed the damping proportional to $\sqrt{c_{\text{imp}}}$ and decaying as $L^{-3/2}$; for overlapped levels we found its $1/L$ dependence. In the "critical" regime of resonant scattering we obtained the parametric enhancement of $1/L$ damping for largest particles and the crossover to the linear-in-L behavior for smallest ones. We examine the possibility to form the phonon-impurity bound state near the phonon band edge for both light and heavy impurities.

VI. DISCUSSION AND INTERMEDIATE CONCLUSIONS

This section is intended to present the discussion of our analytical results elucidating the role of disorder in crystalline nanoparticles. A more complex and detailed summary which includes the comparative analysis of both analytical and numerical approaches to this problem can be found in paper II. In the meantime, two general remarks are in order right now.

First, we would like to point out that in the above consideration we did not present the unified analytical theory of phonons in disordered nanoparticles. Instead, we investigate the important features of this problem by studying several simplest models which probably exaggerate and oversimplify the real experimental situation (cf. paper II). This allows us to extract the characteristic spatial scales associated with these features and, more importantly, to formulate the *qualitative* model-free picture of the phonon-impurity scattering in nanoparticles.

Our second remark is related to the object we addressed in this paper. We would like to emphasize that we evaluated the broadening of *individual lines* in the spectrum of vibrational eigenmodes in nanoparticles of a given shape. Only all these lines treated together, properly broadened, and elaborated with the use of the theory of photon-phonon interaction constitute the Raman peak in real experiments. This approach should be contrasted with the PCM-like theories wherein the linewidth is a single parameter for the entire Raman peak.

We started our analysis from the treatment of the simplest weak pointlike impurities. We observe that there exist two drastically different regimes depending on whether the vibrational eigenmodes are separated or belong to the (quasi)continuum. In particular, for separated levels the phonon damping behaves as $\Gamma_n \propto \sqrt{S}/L^{3/2}$, where L is the particle size and the disorder strength S is a product of the impurity concentration c_{imp} and the squared relative variation of the random parameter of the theory (in our case, atomic mass m). For overlapped levels we find $\Gamma_n \propto S/L$. In the latter case we solve the bulk problem and perform the finite-size quantization only in final formulas. This (definitely, approximate) approach is justified by the evident similarity between the continuous spectra of propagating phonon modes and the ones of plane waves; the difference is supposed to be negligible.

These results were obtained within the on-shell (Lorentzian) approximation. Beyond this approximation the line shape in the overlapped regime is shown to be strongly asymmetric due to the van Hove singularity in the spectrum of optical phonons, whereas in the separated regime it obeys the semicircle law. We also establish simple relations between the linewidths of eigenmodes with different quantum numbers. The dependence of Γ_n on the quantum number of the level is observed to be stronger in the overlapped regime than in the separated one.

Considering a weak smooth disorder with the characteristic length scale σ we obtain the damping at $\sigma \ll L$ similar to the one for pointlike impurities. In the opposite limit $\sigma \gg L$ it is proportional to L in the overlapped regime and saturates as a function of particle size if the levels are separated. Such a behavior of the phonon linewidth for overlapped levels could be understood from the general quantum mechanical picture of fast vs slow particles scattered off the "soft spheres" potential [51].

Finally, we treated the case of strong impurities with low concentration $c_{\text{imp}} \ll 1$ using the T-matrix approach

borrowed from the theory of dirty fermions [52]. We consider the replacement impurities of a single sort to be strong so the effective local potential generated by the mass defect may even exceed the phonon bandwidth. Our main observation concerning separated levels is that the result for damping is almost the same as for the weak-impurities case. The only difference is an additional shift of the maximal optical phonon frequency ω_0. When regarding the damping for overlapped levels we observe the same particle size and concentration dependence as we found for Born impurities with the prefactor enhancement for light impurity atoms, and an extra crossover to the linear-in-L size dependence that occurs in the latter case.

The T-matrix approach allows us to investigate the bound state of a phonon localized on the impurity. The wave functions of phonons localized in the depth of a particle rapidly decay with the distance and barely feel the particle boundary. Neglecting all boundary effects we analyze the bound states within the bulk approach (or in the overlapped regime). For the light impurities these bound states just above ω_0 appear starting from some threshold value $U_{\min} < 0$ of the impurity potential, whereas heavy atoms may create a bound state only inside the gap between optical and acoustic phonon branches. When the impurity potential $U \to U_{\min}$, the phenomenon of the resonant impurity scattering arises and drastically enhances the long-wavelength phonon damping.

Now let us discuss how the separated and the overlapped regimes cross over. Since the linewidth depends (among other things) on the quantum number of a level (both directly and via the particle shape), various parts of the spectrum may simultaneously exist in different regimes. Information about this dependence could be extracted either from the analytical calculations or (for nontrivial particle shapes) from the numerical simulations. In order to identify the regime of broadening for any couple of spectral lines one should compare the interlevel distance and the sum of half-widths for these lines, i.e.,

$$\omega_{n+1} - \omega_n = \tfrac{1}{2}\,[\,\Gamma_{n+1} + \Gamma_n\,]. \tag{70}$$

Notice that Γ_n and Γ_{n+1} could be in different regimes if say the levels ω_{n-1} and ω_n are already overlapped while ω_n and ω_{n+1} are not.

Next, since the linewidths in different regimes reveal different size and disorder dependencies, it is instructive to determine the characteristic size for these two quantities to be equal to each other. Dropping the coefficients one obtains

$$\mathcal{L}_c \sim \frac{a_0}{S}. \tag{71}$$

Remarkably, the linewidth (in both regimes) reaches the interlevel distance on the same scale. In different terms, $\mathcal{L}_c$ is the spatial scale for the ballistic Thouless time [53] (the time for a phonon to fly ballistically through the particle) and the phonon lifetime $1/\Gamma_n$ to coincide. Moreover, Eq. (71) can be inverted, thus determining the critical disorder strength for a given particle size

$$\mathcal{S}_c \sim \frac{a_0}{L}. \tag{72}$$

ACKNOWLEDGMENTS

The authors are thankful to Igor Gornyi for valuable comments. This work is supported by the Russian Science Foundation (Grant No. 19-72-00031).

APPENDIX: DISORDER IN EKFG FORMALISM

The consideration given in the main body of this paper is presented in a maximally general form applicable for both theories (DMM-BPM, EKFG) that we developed. This provides the limitations on the final results including the coefficients and some relevant dependencies. In this Appendix we illustrate how the problem can be solved to the end for some particular case. As an example we choose the EKFG theory of a cubic particle which could be treated analytically. Since the overlapped regime is trivial we concentrate on the regime of separated levels.

1. Hamiltonian and quantization

We start from the Hamiltonian of the EKFG model:

$$\mathcal{H}_0 = \frac{1}{2}\int_\Omega d^3\mathbf{r}[\Pi^2 - C_1(\nabla\Phi)^2 + C_2\Phi^2]. \tag{A1}$$

Here the quantized field in the Schrödinger representation

$$\Phi(\mathbf{r}) = \sum_n \frac{1}{\sqrt{2\omega_n}}[b_n Y_n(\mathbf{r}) + b_n^+ Y_n^*(\mathbf{r})] \tag{A2}$$

and momentum operator

$$\Pi(\mathbf{r}) = -\sum_n i\sqrt{\frac{\omega_n}{2}}[b_n Y_n(\mathbf{r}) - b_n^+ Y_n^*(\mathbf{r})] \tag{A3}$$

are expressed via the phonon creation-annihilation operators b_n^+ (b_n) and the eigenfunctions of the EKFG model Y_n. They obey conventional commutation relation

$$[\Phi(\mathbf{r}), \Pi(\mathbf{r}')] = -i\delta(\mathbf{r} - \mathbf{r}'). \tag{A4}$$

It is easy to show that the quantized Hamiltonian reads

$$\mathcal{H}_0 = \sum_n \omega_n(b_n^+ b_n + 1/2). \tag{A5}$$

Next, we can define the causal phonon Green's function

$$D(\mathbf{r}_1, t_1, \mathbf{r}_2, t_2) = -i\langle 0|\hat{\mathrm{T}}(\Phi(\mathbf{r}_1, t_1)\Phi(\mathbf{r}_2, t_2))|0\rangle. \tag{A6}$$

After simple calculations and Fourier transform we get

$$D_0(\mathbf{r}_1, \mathbf{r}_2, \omega) = \sum_n \frac{Y_n(\mathbf{r}_1)Y_n(\mathbf{r}_2)}{\omega^2 - \omega_n^2 + i0}, \tag{A7}$$

where the eigenfunctions Y_n are real.

Considering the solution of Eq. (2) for a given frequency ω we obtain

$$(\omega^2 - C_1)Y - C_2\triangle Y = 0. \tag{A8}$$

First, we should solve the eigenproblem

$$\Delta Y + q^2 Y = 0, \quad Y|_{\partial\Omega} = 0, \tag{A9}$$

where q will be referred to as the momentum. Thus, the spectrum of the problem has the form

$$\omega_{\mathbf{q}}^2 = C_2 - C_1 q^2. \tag{A10}$$

This is the equivalent of Eq. (21):

$$\omega_{\mathbf{q}} = \omega_0 - \alpha q^2, \tag{A11}$$

where we put $\omega_0 = \sqrt{C_2}$ and $\alpha = C_1/(2\sqrt{C_2})$.

As an example we consider the cubic nanoparticle with the edge b. In that case the EKFG equation has obvious solutions normalized to unity:

$$Y_{\mathbf{n}} = \left(\frac{2}{b}\right)^{3/2} e^{-i\omega t} \sin\frac{\pi n_x x}{b} \sin\frac{\pi n_y y}{b} \sin\frac{\pi n_z z}{b}, \tag{A12}$$

where the vector $\mathbf{n} = (n_x, n_y, n_z)$ enumerates the eigenstates, and the eigenvalues are

$$\omega_{\mathbf{n}} = \omega_0 - \alpha\left(\frac{\pi}{b}\right)^2\left(n_x^2 + n_y^2 + n_z^2\right). \tag{A13}$$

2. Pointlike impurities

The variation of atomic masses in the lattice model corresponds to the variation of parameters $C_{1,2}$ of Eq. (A1) in the continuous model. In the range of EKFG validity $q\,a_0 \ll 1$ we can neglect the variation of C_1. Thus, the disorder-induced perturbation of the Hamiltonian reads

$$\delta\mathcal{H} = \frac{1}{2}\int_\Omega d^3\mathbf{r}[C_2(\mathbf{r}) - \overline{C_2}]\Phi^2. \tag{A14}$$

Here $\overline{C_2} = \omega_0^2$ stands for the average value of $C_2(\mathbf{r})$. Evidently, $C_2(\mathbf{r}) - \overline{C_2} \approx -\omega_0^2\delta m(\mathbf{r})/m$, and we can write

$$\delta\mathcal{H} = -\frac{1}{4}\sum_{n,n'}\int_\Omega d^3\mathbf{r}\,\frac{\omega_0^2}{\sqrt{\omega_n\omega_{n'}}}\frac{\delta m(\mathbf{r})}{m} \times (b_n + b_n^+)(b_{n'} + b_{n'}^+)Y_n(\mathbf{r})Y_{n'}(\mathbf{r}). \tag{A15}$$

Within the EKFG approximation the disorder correlation function for weak pointlike impurities is given by

$$\frac{\langle\delta m(\mathbf{r}_1)\,\delta m(\mathbf{r}_2)\rangle}{m^2} = S\,V_0\,\delta(\mathbf{r}_1 - \mathbf{r}_2), \tag{A16}$$

where V_0 is the unit cell volume.

In the limit of weak impurities only the second diagram in Fig. 4(b) is relevant. By virtue of Eq. (A16) the correction to the phonon Green's function yields

$$\delta D(\mathbf{r}_1, \mathbf{r}_2, \omega) = \frac{SV_0\omega_0^4}{4}\int d^3\mathbf{r}\left[\sum_n \frac{Y_n(\mathbf{r}_1)Y_n(\mathbf{r})}{\omega^2 - \omega_n^2 + i0} \times \sum_{n'}\frac{Y_{n'}(\mathbf{r})Y_{n'}(\mathbf{r})}{\omega^2 - \omega_{n'}^2 + i0}\sum_{n''}\frac{Y_{n''}(\mathbf{r})Y_{n''}(\mathbf{r}_2)}{\omega^2 - \omega_{n''}^2 + i0}\right]. \tag{A17}$$

For further analysis it is useful to perform the discrete Fourier transform of equation

$$D(\mathbf{r}_1, \mathbf{r}_2, \omega) = D_0(\mathbf{r}_1, \mathbf{r}_2, \omega) + \delta D(\mathbf{r}_1, \mathbf{r}_2, \omega). \tag{A18}$$

In order to execute this transformation we multiply Eq. (A18) by $Y_n(\mathbf{r}_1)Y_n(\mathbf{r}_2)$ and integrate it over $\mathbf{r}_1$ and $\mathbf{r}_2$. This procedure eliminates the sum in Eq. (A7) and sums over n and n'' in Eq. (A17) due to the orthogonality of eigenfunctions Y_n. We can rewrite Eq. (A18) introducing the renormalized complex eigenfrequencies $\tilde{\omega}_n$ as follows:

$$\omega^2 - \tilde{\omega}_n^2 = \omega^2 - \omega_n^2 - \Pi_n(\omega), \tag{A19}$$

where

$$\Pi_n(\omega) = \frac{S\,V_0\,\omega_0^4}{4}\int d^3\mathbf{r}\sum_{n'}\frac{Y_n^2(\mathbf{r})Y_{n'}^2(\mathbf{r})}{\omega^2 - \omega_{n'}^2 + i0}. \tag{A20}$$

Using the eigenfunctions (A12) we can calculate the self-energy (A20):

$$\Pi_n(\omega) = \frac{S\,V_0\,\omega_0^4}{32\,V}\sum_{\mathbf{n}'}\frac{\prod_{i=x,y,z}(2 + \delta_{n_i n_i'})}{\omega^2 - \omega_{\mathbf{n}'}^2 + i0}, \tag{A21}$$

where V is the particle volume. We find the phonon damping analytically using the self-consistent approach and the isolated-levels approximation:

$$\Pi_{\mathbf{n}}(\omega) = \frac{27\,S\,V_0\,\omega_0^4}{32\,V}\frac{1}{\omega^2 - \omega_{\mathbf{n}}^2 - \Pi_{\mathbf{n}}(\omega)}. \tag{A22}$$

Solving this equation, we obtain

$$\Pi_{\mathbf{n}}(\omega) = \frac{(\omega^2 - \omega_{\mathbf{n}}^2) - \sqrt{(\omega^2 - \omega_{\mathbf{n}}^2)^2 - 4\frac{27S\omega_0^4}{32N}}}{2}. \tag{A23}$$

The phonon line obeys the semicircle law (see Fig. 5), and the width of the phonon line is given by

$$\Gamma_{\mathbf{n}} = \omega_0\sqrt{\frac{27S}{32N}}. \tag{A24}$$

For a degenerate level $\mathbf{n}$ only the coefficient in Eq. (A24) should be modified. If two quantum numbers in $\mathbf{n}$ are equal to each other then the level is threefold degenerate and instead of $27/32$ we get $(27 + 24)/32 = 51/32$. For a sixfold-degenerate level with all three quantum numbers different the multiplier is $79/32$.

Furthermore, from Eq. (A21) one can find the real part of the correction. This contribution is proportional to S.

Finally, from Eq. (A24) we precisely determine the characteristic crossover scale $\mathcal{L}_c$ for the first level:

$$\mathcal{L}_c = 15\pi^4 F^2\frac{a_0}{S}. \tag{A25}$$

For a diamond $F \approx 0.008$, and the prefactor in front of the model-free ratio in Eq. (A25) is not too small ($\approx$0.093).

3. Smooth disorder

Now we consider a smooth Gaussian disorder with certain characteristic length scale σ. The correlator reads

$$\frac{\langle\delta m(\mathbf{r}_1)\delta m(\mathbf{r}_2)\rangle}{m^2} = \frac{S}{\sigma^3(2\pi)^{3/2}}e^{-(\mathbf{r}_1 - \mathbf{r}_2)^2/2\sigma^2}. \tag{A26}$$

Using this correlator we obtain the following correction to the phonon Green's function:

$$\delta D(\mathbf{r}_1,\mathbf{r}_2,\omega)=\frac{S\,\omega_0^4}{4}\int d^3\mathbf{r}d^3\mathbf{r}'\left[\sum_n\frac{Y_n(\mathbf{r}_1)Y_n(\mathbf{r})}{\omega^2-\omega_n^2+i0}\sum_{n'}\frac{Y_{n'}(\mathbf{r})Y_{n'}(\mathbf{r}')}{\omega^2-\omega_{n'}^2+i0}\sum_{n''}\frac{Y_{n''}(\mathbf{r}')Y_{n''}(\mathbf{r}_2)}{\omega^2-\omega_{n''}^2+i0}\right]\frac{e^{-(\mathbf{r}-\mathbf{r}')^2/2\sigma^2}}{\sigma^3(2\pi)^{3/2}}.$$

For nondegenerate level $\mathbf{n}$ and $q_{\mathbf{n}}^2\sigma^2\ll 1$ we have only a small correction to the damping:

$$\Gamma_{\mathbf{n}}=\omega_0\sqrt{\frac{27\,S}{32\,N}\left(1-\frac{2}{3}q_{\mathbf{n}}^2\sigma^2\right)}. \tag{A27}$$

For the threefold-degenerate level the damping reads

$$\Gamma_{\mathbf{n}}=\omega_0\sqrt{\frac{\left(51-42\,\frac{\pi^2n_x^2\sigma^2}{b^2}-76\,\frac{\pi^2n_y^2\sigma^2}{b^2}\right)S}{32N}}, \tag{A28}$$

and for the sixfold one the result is as follows:

$$\Gamma_{\mathbf{n}}=\omega_0\sqrt{\frac{(79-66\,q_{\mathbf{n}}^2\sigma^2)S}{32\,N}}. \tag{A29}$$

Thus, at $q_{\mathbf{n}}^2\sigma^2\ll 1$ the smooth random potential yields almost the same result as the pointlike impurities. For first modes with highest frequencies this condition is equivalent to $\sigma\ll L$; i.e., the length scale of the random potential must be much smaller than the particle size.

[1] K. D. Behler, A. Stravato, V. Mochalin, G. Korneva, G. Yushin, and Y. Gogotsi, ACS Nano **3**, 363 (2009).

[2] P. Andrich, F. Charles, X. Liu, H. L. Bretscher, J. R. Berman, F. J. Heremans, P. F. Nealey, and D. D. Awschalom, npj Quantum Inf. **3**, 28 (2017).

[3] M. Veldhorst, J. Hwang, C. Yang, A. Leenstra, B. de Ronde, J. Dehollain, J. Muhonen, F. Hudson, K. Itoh, A. Morello *et al.*, Nat. Nanotechnol. **9**, 981 (2014).

[4] D. Riedel, I. Söllner, B. J. Shields, S. Starosielec, P. Appel, E. Neu, P. Maletinsky, and R. J. Warburton, Phys. Rev. X **7**, 031040 (2017).

[5] Y. Xia, H. Yang, and C. T. Campbell, Acc. Chem. Res. **46**, 1671 (2013).

[6] Y. Lin, X. Sun, D. S. Su, G. Centi, and S. Perathoner, Chem. Soc. Rev. **47**, 8438 (2018).

[7] O. Faklaris, V. Joshi, T. Irinopoulou, P. Tauc, M. Sennour, H. Girard, C. Gesset, J.-C. Arnault, A. Thorel, J.-P. Boudou *et al.*, ACS Nano **3**, 3955 (2009).

[8] S. E. Kim, L. Zhang, K. Ma, M. Riegman, F. Chen, I. Ingold, M. Conrad, M. Z. Turker, M. Gao, X. Jiang *et al.*, Nat. Nanotechnol. **11**, 977 (2016).

[9] M. A. Walling, J. A. Novak, and J. R. Shepard, Int. J. Mol. Sci. **10**, 441 (2009).

[10] L.-L. Li, K.-P. Liu, G.-H. Yang, C.-M. Wang, J.-R. Zhang, and J.-J. Zhu, Adv. Funct. Mater. **21**, 869 (2011).

[11] V. Pichot, M. Comet, E. Fousson, C. Baras, A. Senger, F. Le Normand, and D. Spitzer, Diam. Relat. Mater. **17**, 13 (2008).

[12] A. Dideikin, A. Aleksenskii, M. Baidakova, P. Brunkov, M. Brzhezinskaya, V. Y. Davydov, V. Levitskii, S. Kidalov, Y. A. Kukushkina, D. Kirilenko *et al.*, Carbon **122**, 737 (2017).

[13] S. Stehlik, M. Varga, M. Ledinsky, V. Jirasek, A. Artemenko, H. Kozak, L. Ondic, V. Skakalova, G. Argentero, T. Pennycook, J. C. Meyer, A. Fejfar, A. Kromka, and B. Rezek, J. Phys. Chem. C **119**, 27708 (2015).

[14] S. Stehlik, M. Varga, M. Ledinsky, D. Miliaieva, H. Kozak, V. Skakalova, C. Mangler, T. J. Pennycook, J. C. Meyer, A. Kromka *et al.*, Sci. Rep. **6**, 38419 (2016).

[15] M. Skapas, S. Stanionytė, T. Paulauskas, and R. Butkutė, Phys. Status Solidi (b) **256**, 1800365 (2019).

[16] A. Pandey and P. Guyot-Sionnest, Science **322**, 929 (2008).

[17] S. Osswald, V. N. Mochalin, M. Havel, G. Yushin, and Y. Gogotsi, Phys. Rev. B **80**, 075419 (2009).

[18] A. D. Trofimuk, D. V. Muravijova, D. A. Kirilenko, and A. V. Shvidchenko, Materials **11**, 1285 (2018).

[19] R. Pecora, J. Nanopart. Res. **2**, 123 (2000).

[20] S. Koniakhin, I. Eliseev, I. Terterov, A. Shvidchenko, E. Eidelman, and M. Dubina, Microfluid. Nanofluid. **18**, 1189 (2015).

[21] E. Ōsawa, Pure Appl. Chem. **80**, 1365 (2008).

[22] S. V. Koniakhin, M. K. Rabchinskii, N. A. Besedina, L. V. Sharonova, A. V. Shvidchenko, and E. D. Eidelman, Phys. Rev. Res. **2**, 013316 (2020).

[23] S. Koniakhin, N. Besedina, D. Kirilenko, A. Shvidchenko, and E. Eidelman, Superlattices Microstruct. **113**, 204 (2018).

[24] O. A. Shenderova, I. I. Vlasov, S. Turner, G. Van Tendeloo, S. B. Orlinskii, A. A. Shiryaev, A. A. Khomich, S. N. Sulyanov, F. Jelezko, and J. Wrachtrup, J. Phys. Chem. C **115**, 14014 (2011).

[25] V. I. Korepanov, J. Raman Spectrosc. **51**, 881 (2020).

[26] S. V. Koniakhin, O. I. Utesov, I. N. Terterov, A. V. Siklitskaya, A. G. Yashenkin, and D. Solnyshkov, J. Phys. Chem. C **122**, 19219 (2018).

[27] O. I. Utesov, A. G. Yashenkin, and S. V. Koniakhin, J. Phys. Chem. C **122**, 22738 (2018).

[28] H. Richter, Z. Wang, and L. Ley, Solid State Commun. **39**, 625 (1981).

[29] I. Campbell and P. M. Fauchet, Solid State Commun. **58**, 739 (1986).

[30] J. Zi, K. Zhang, and X. Xie, Phys. Rev. B **55**, 9263 (1997).
[31] G. Faraci, S. Gibilisco, P. Russo, A. R. Pennisi, and S. La Rosa, Phys. Rev. B **73**, 033307 (2006).
[32] V. I. Korepanov, H. Hamaguchi, E. Osawa, V. Ermolenkov, I. K. Lednev, B. J. Etzold, O. Levinson, B. Zousman, C. P. Epperla, and H.-C. Chang, Carbon **121**, 322 (2017).
[33] W. Ke, X. Feng and Y. Huang, J. App. Phys. **109**, 083526 (2011).
[34] Y. Gao and P. Yin, Diam. Relat. Mater. **99**, 107524 (2019).
[35] A. Meilakhs and S. Koniakhin, Superlattices Microstruct. **110**, 319 (2017).
[36] L. Landau and E. Lifshitz, *Mechanics: Volume 1* (Elsevier Science, Oxford, UK, 1982).
[37] A. Jorio, M. Dresselhaus, R. Saito, and G. Dresselhaus, *Raman Spectroscopy in Graphene Related Systems* (Wiley, 2011).
[38] M. Yoshikawa, Y. Mori, M. Maegawa, G. Katagiri, H. Ishida, and A. Ishitani, Appl. Phys. Lett. **62**, 3114 (1993).
[39] S. V. Koniakhin, O. I. Utesov, and A. G. Yashenkin, Phys. Rev. B **102**, 205422 (2020).
[40] A. G. Yashenkin, O. I. Utesov, and S. V. Koniakhin, arXiv:2004.12631.
[41] M. Born and K. Huang, *Dynamical Theory of Crystal Lattices* (Clarendon Press, Oxford, 1954).
[42] P. Keating, Phys. Rev. **145**, 637 (1966).
[43] Mathematica, *Version 11.0*, Wolfram Research, Inc., Champaign, Illinios, 2010.
[44] J. W. Ager, D. K. Veirs, and G. M. Rosenblatt, Phys. Rev. B **43**, 6491 (1991).
[45] S. V. Koniakhin, O. I. Utesov, I. N. Terterov, and A. V. Nalitov, Phys. Rev. B **95**, 045418 (2017).
[46] A. Abrikosov, L. Gorkov, I. Dzyaloshinski, and R. Silverman, *Methods of Quantum Field Theory in Statistical Physics*, Dover Books on Physics (Dover Publications, New York, 2012).
[47] T. Ando and Y. Uemura, J. Phys. Soc. Jpn. **36**, 959 (1974).
[48] M. Stone, *Quantum Hall Effect* (World Scientific, Singapore, 1992).
[49] L. Landau and E. Lifshitz, *Statistical Physics: Volume 5* (Elsevier Science, Oxford, 2013).
[50] B. P. Toperverg and A. G. Yashenkin, Phys. Rev. B **48**, 16505 (1993).
[51] L. Landau and E. Lifshitz, *Quantum Mechanics: Non-Relativistic Theory* (Elsevier Science, Oxford, 2013).
[52] S. Doniach and E. Sondheimer, *Green's Functions for Solid State Physicists* (Imperial College Press, London, 1998).
[53] J. T. Edwards and D. J. Thouless, J. Phys. C **5**, 807 (1972).